Biomaterials Science

ROYAL SOCIETY OF CHEMISTRY

PAPER

View Article Online
View Journal | View Issue

Cite this: *Biomater. Sci.*, 2024, **12**, 3335

A chlorogenic acid-conjugated nanomicelle attenuates disease severity in experimental arthritis†

Akshay Vyawahare,[a] Chandrashekhar Jori,[a] Jattin Kumar,[a] Kanika,[a] Mohammad Fareed,[b] Nemat Ali,[c] Kaushik Parida [d] and Rehan Khan *[a]

Rheumatoid arthritis (RA) is a systemic immune disorder marked by synovitis, bone damage, and cartilage erosion, leading to increased socio-economic burdens and reduced quality of life. Despite its unknown cause, advancements in understanding its pathophysiology have facilitated novel therapeutic approaches. Current treatments, including disease-modifying anti-rheumatic drugs (DMARDs) and biologics, often result in low efficacy and unnecessary side effects. To address the limitations of these drugs, carrier-based drug delivery systems, such as nanomicelles, have emerged as a promising solution. In this study, nanomicelles were synthesised utilizing PLGA (poly(lactic-*co*-glycolic acid)) as a backbone; this backbone is conjugated with chlorogenic acid (CGA), which is known for suppressing inflammation, and incorporates methotrexate (MTX), a model drug that is established for RA treatment. The nanomicelles were extensively characterized in terms of size, charge, drug loading, and drug-release behaviour. The *in vivo* assessment of MTX-PLGA-*b*-CGA nanomicelles in a collagen-induced arthritis model demonstrated a remarkable reduction in joint swelling, cartilage erosion, and disease severity. Furthermore, histological findings confirmed cartilage integrity and reduced expression of key pro-inflammatory markers, including receptor activator of nuclear factor kappa beta ligand (RANKL) and tumor necrosis factor (TNF-α). The approach based on the MTX-PLGA-*b*-CGA nanomicelles presents a biocompatible and potentially effective therapeutic strategy for management of the severity and progression of RA, providing a hopeful alternative for RA treatment.

Received 29th December 2023,
Accepted 8th May 2024

DOI: 10.1039/d3bm02129g

rsc.li/biomaterials-science

Introduction

Rheumatoid arthritis (RA) is a systemic immune disorder characterized by synovitis, bone damage and cartilage erosion.[1,2] It is estimated that RA affects 0.5–1% of the population globally. The disease complexation is associated with socioeconomic cost, immobility, disability and early death. The etiological factors responsible for the RA disease development are still ambiguous.[3,4] Furthermore, progress in understanding its pathophysiology has fostered new strategies to mitigate the disease severity.

The exact origin of RA is still unknown, although there are a number of likely explanations for how it develops, including genetic abnormalities, hormonal changes, microbial infections, exposure to metals, and aberrant immunological responses.[5,6] The current focus of clinical procedures for managing RA is on symptomatic therapies, bone and joint damage minimization, and pain relief.[7] Numerous pro-inflammatory cytokines, including interleukins, tumour necrosis factor-alpha (TNF-α), and regulators for receptor activator nuclear factor-κB ligand (RANKL), are important mediators in the pathophysiology of RA.[8,9] Additional inflammatory cells are further mobilized and activated by these cytokines, which cause them to infiltrate and generate enzymes that break down bone and cartilage.[10] The current standard of care for RA is the use of disease-modifying antirheumatic drugs (DMARDs), nonsteroidal anti-inflammatory medications (NSAIDs), and corticosteroids, but these medications come with many drawbacks and side effects, such as low bioavailability and the need to enhance drug efficacy while minimizing systemic side

[a]*Chemical Biology Unit, Institute of Nano Science and Technology (INST), Knowledge City, Sector-81, Mohali-140306, Punjab, India. E-mail: rehankhan@inst.ac.in; Tel: +91-172-2210075extn: 7030*
[b]*Centre for Global Health Research, Saveetha Institute of Medical and Technical Sciences, Saveetha University, Chennai, Tamil Nadu, India*
[c]*Department of Pharmacology & Toxicology, College of Pharmacy, King Saud University, Riyadh 11451, Saudi Arabia*
[d]*Department of Polymer and Process Engineering, Indian Institute of Technology, Roorkee 247667, Uttarakhand, India*

† Electronic supplementary information (ESI) available. See DOI: https://doi.org/10.1039/d3bm02129g

effects.[11–13] Furthermore, conventional therapies are not able to provide a perfect cure.[14,15] These constraints hinder therapeutic outcomes and need to be addressed through the designing of a nanocarrier-based drug delivery system. Nanomicelle drug delivery systems have emerged as promising drug delivery systems for the delivery of hydrophobic or potent drugs to site of inflammation.[16,17] Based on the O2-economized dual energy inhibition technique, the smart nanoplatform (V-HAGC) and H_2O_2/NIR have been used to accomplish increased CDT (chemodynamic treatment), PTT (photothermal therapy), and photodynamic therapy of RA.[18–20]

In this work, we created a nanomicelle made of biocompatible poly(lactic-*co*-glycolic acid)(PLGA) coupled to active natural compound chlorogenic acid (CGA), which inhibits inflammation and inflammation-related mediators, including TNF-α, IL-1β, and NF-κB.[21,22] Additionally, we included the promising medication methotrexate (MTX), which is commonly prescribed to treat RA. By inhibiting the production of osteoclast precursors (OCPs), which release pro-inflammatory cytokines, MTX reduces joint inflammation by blocking the receptor activator nuclear factor-κB ligand (RANKL).[23] We proposed that MTX-loaded PLGA-*b*-CGA, (MTX-PLGA-*b*-CGA) nanomicelles show esterase-responsiveness and thus CGA will be released upon breakage of ester bonds, thus both MTX and CGA will act as a therapeutic drug, leading to additive suppression of the pro-inflammatory markers, which contributes to prevention and inhibition of disease progression.

We investigated the therapeutic efficacy of MTX-PLGA-*b*-CGA in collagen-induced arthritis (CIA) in Wistar rats. Our findings demonstrate a significant reduction in joint swelling, cartilage erosion, and disease severity following treatment, as evidenced by physiological, X-ray, and histological assessments. Immunohistochemical analysis revealed downregulation of the pro-inflammatory markers RANKL and TNF-α after MTX-PLGA-*b*-CGA treatment, suggesting its potential in mitigating joint inflammation. Additionally, the biocompatibility of the MTX-PLGA-*b*-CGA nanomicelles underscores their promise as an alternative therapeutic approach for managing rheumatoid arthritis.

Results

Synthesis and characterization of PLGA-*b*-CGA nanomicelles

We synthesized chlorogenic acid-conjugated PLGA (PLGA-*b*-CGA) nanomicelles through esterification in the presence of DCC and 4-DMAP (4-dimethylaminopyridine) (Fig. 1B) following a protocol modified from ref. 24. The self-assembly of the MTX-loaded nanomicelle is depicted in Fig. 1A. The reaction was optimized and characterized using first ^{1}H-NMR and later IR spectroscopy. The following characteristic protons of PLGA were observed: $-CH_3$ at δ = 1.47 ppm, –CH– at δ = 5.09 ppm, O═CHO at δ = 4.86–4.91 ppm. The observed protons of PLGA were as follows: aromatic $-CH_2$ at δ = 1.95 ppm, aromatic –CH– at δ = 3.53–3.55 ppm, aromatic –CH– δ = 3.91 ppm, aromatic –OH δ = 4.06 ppm, aromatic $-CH_2-$ at δ = 2.26 ppm, ═CH– at δ = 6.15–6.19 ppm, ═CH– at δ = 7.40–7.44 ppm, aromatic ═CH═ at δ = 6.98–7.01 ppm, aromatic –OH– at δ = 8.14 ppm, aromatic ═CH═ at δ = 6.76–6.78 ppm, aromatic δ = 6.71 ppm, as depicted in Fig. 1G. Further, we compared the IR spectra of each compound with those of its conjugated and drug-loaded forms. Briefly, we observed a characteristic peak of PLGA, specifically, the –C═O stretch, at 1750 cm^{-1}; similarly, chlorogenic acid showed a –C═O stretch at 1691 cm^{-1}. The conjugated form of PLGA-*b*-CGA showed a characteristic ester stretch at 1750 cm^{-1} and –COOH stretch at 3350 cm^{-1} and –CH stretch at 2929–2856 cm^{-1}. Methotrexate (MTX) showed characteristic bands related to the amine group at 1536 cm^{-1} and aromatic –C═C═ vibrations at 1400 cm^{-1}. Furthermore, characteristic spectra for MTX-loaded PLGA-*b*-CGA showed all the characteristic peaks of conjugated and drug-loaded forms, and all the characteristic peaks have been matched and labelled in Fig. 1C. Further, we assessed PLGA-*b*-CGA self-assembly and the formation of the nanomicelles. First, we characterized their hydrodynamic diameter using dynamic light scattering (DLS), and found it to be around 80–95 nm for PLGA-*b*-CGA, whereas after the incorporation of MTX, the hydrodynamic diameter increased to around 110–125 nm (Fig. 1D). The nanomicelles are in the nanometer range, which is optimum for uptake into synoviocytes or synovial cells present in the inflamed synovium. The maximum threshold uptake depends upon the size of the nanoparticle, which should be less than 400 nm. We then measured the zeta potential of PLGA-*b*-CGA and MTX-loaded PLGA-*b*-CGA to analyze their surface charges, which were observed around −5 mV and −9 mV, respectively (Fig. 1E). The negative charge is due to the presence of acidic acetate groups, which are negatively charged. Furthermore, the PLGA-*b*-CGA and MTX-loaded PLGA-*b*-CGA nanomicelles were visualized using transmission electron microscopy (TEM) to determine their shape, morphology and size. We observed the MTX-loaded PLGA-*b*-CGA nanomicelles to be ball-shaped with a size of around 100–125 nm from the TEM micrograph (Fig. 1F). The ball-shaped nanomicelles have several advantages, such as making internalization, endocytosis and blood circulation faster.[25,26]

We further assessed the release of MTX from the PLGA-*b*-CGA nanomicelles. The drug release study was performed to qualitatively and quantitatively assess the potential of the nanomicelle to release the drug under different pH and enzymatic conditions. The retention time and release pattern were also assessed in the *in vitro* drug release study. This gave us an idea of how the nano-formulation would behave with respect to joint retention time when administered in disease conditions. We initially calculated the drug loading and encapsulation efficiency of MTX, which were observed to be 28.23% and 85%, respectively. We performed the *in vitro* drug release study using the conventional dialysis bag method.[22,23] A known amount of MTX-PLGA-*b*-CGA was immersed in 2 ml of PBS (pH 7.4) and dispersed in a dialysis bag with a molecular weight cut-off of 12 kDa. The dialysis bag was clipped at both ends and stirred in 250 mL of PBS (pH 7.4) for particular time.

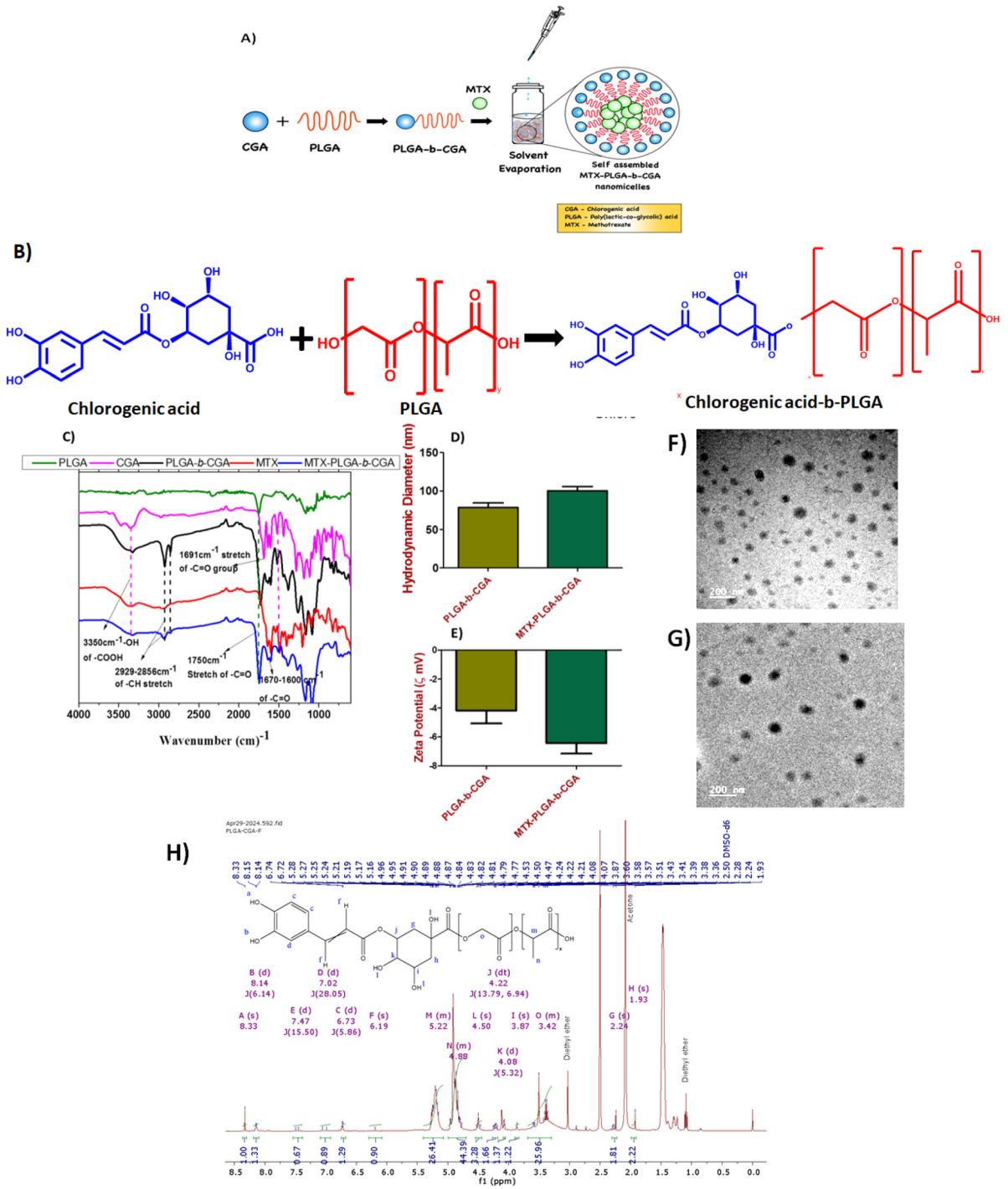

Fig. 1 Representative images and graphs for the synthesis and characterization of the nanomicelle. (A) Representation of the self-assembly of the MTX-loaded nanomicelles in water. (B) Synthetic scheme for the conjugation of the PLGA-*b*-CGA nanomicelles. (C) FTIR spectrum analysis of conjugated and MTX-loaded PLGA-*b*-CGA. (D) Hydrodynamic diameter of blank PLGA-*b*-CGA as well as MTX-PLGA-*b*-CGA. (D and E) Surface zeta potential of PLGA-*b*-CGA and MTX-PLGA-*b*-CGA. (F) TEM imaging of MTX-PLGA-*b*-CGA. (F and G) TEM imaging of PLGA-*b*-CGA and MTX-PLGA-*b*-CGA. (H) ^{1}H-NMR spectra of synthesized PLGA-*b*-CGA conjugate. Values are given as mean ± s.d. $n = 3$.

We collected a 1 mL sample at intervals of 0 min, 30 min, 1 h, 2 h, 4 h, 8 h, 16 h, 24 h, 36 h, and 48 h. The sink condition was maintained by adding back 1 mL of PBS. We then scanned the sample using UV-Vis spectrometry to measure the maximum absorbance at a λ_{max} of ~303 nm for MTX. The concentration of MTX released at a particular time was calculated by interpolation with a calibration curve of MTX. We initially observed slow release at times of up to 4 h; increased release

was observed at 8 h, at which 40% of the MTX had been released, and then, MTX was released in a sustained manner up to 48 h, at which time 65% of the MTX had been released (Fig. 2A). We further assessed the MTX release in presence of inflammatory conditions (pH 5.8 + esterase). We observed that the inflammatory pH and presence of esterase triggered the release of MTX, as esterase is abundant in inflammatory conditions and further disassembled the nanomicelles to trigger the drug release. At 8 h, we observed that 60% of the MTX had been released, and the MTX release was sustained to reach 82% at 48 h. The triggered release was observed due to the esterase-cleavable structure. Furthermore, the study involved the assessment of the release of CGA from the nanomicelle assembly. We performed the release in PBS (pH 7.4) and at the inflammatory pH of 5.8 in the presence of the enzyme esterase. We observed that the release of CGA was lower or negligible in the case of PBS (pH 7.4), whereas the release was significantly higher or triggered in the pH 5.8 and esterase conditions. The reason for the triggered release was that the esterase present cleaved the ester bond assembly between the PLGA and CGA; hence, this process occurs simultaneously with MTX release (Fig. 2A).

We further assessed the cytocompatibility or biocompatibility through *in vitro* assessment on healthy human hTERT-BJ cells.[27,28] We used XTT (2,3-bis-(2-methoxy-4-nitro-5-sulfophenyl)-2*H*-tetrazolium-5-carboxanilide) assay for the evaluation of cytocompatibility in healthy cells. Various concentrations ranging from 1.95 μg mL^{-1} to 500 μg mL^{-1} of MTX-PLGA-*b*-CGA were incubated on 1×10^4 cells per well. The cell viability was measured by comparing the intensity of each observation with the control group. We observed that formulated MTX-PLGA-*b*-CGA concentrations were highly cytocompatible and showed no cytotoxicity at concentrations of up to 250 μg mL^{-1}. We also noted a non-significant change in cell viability

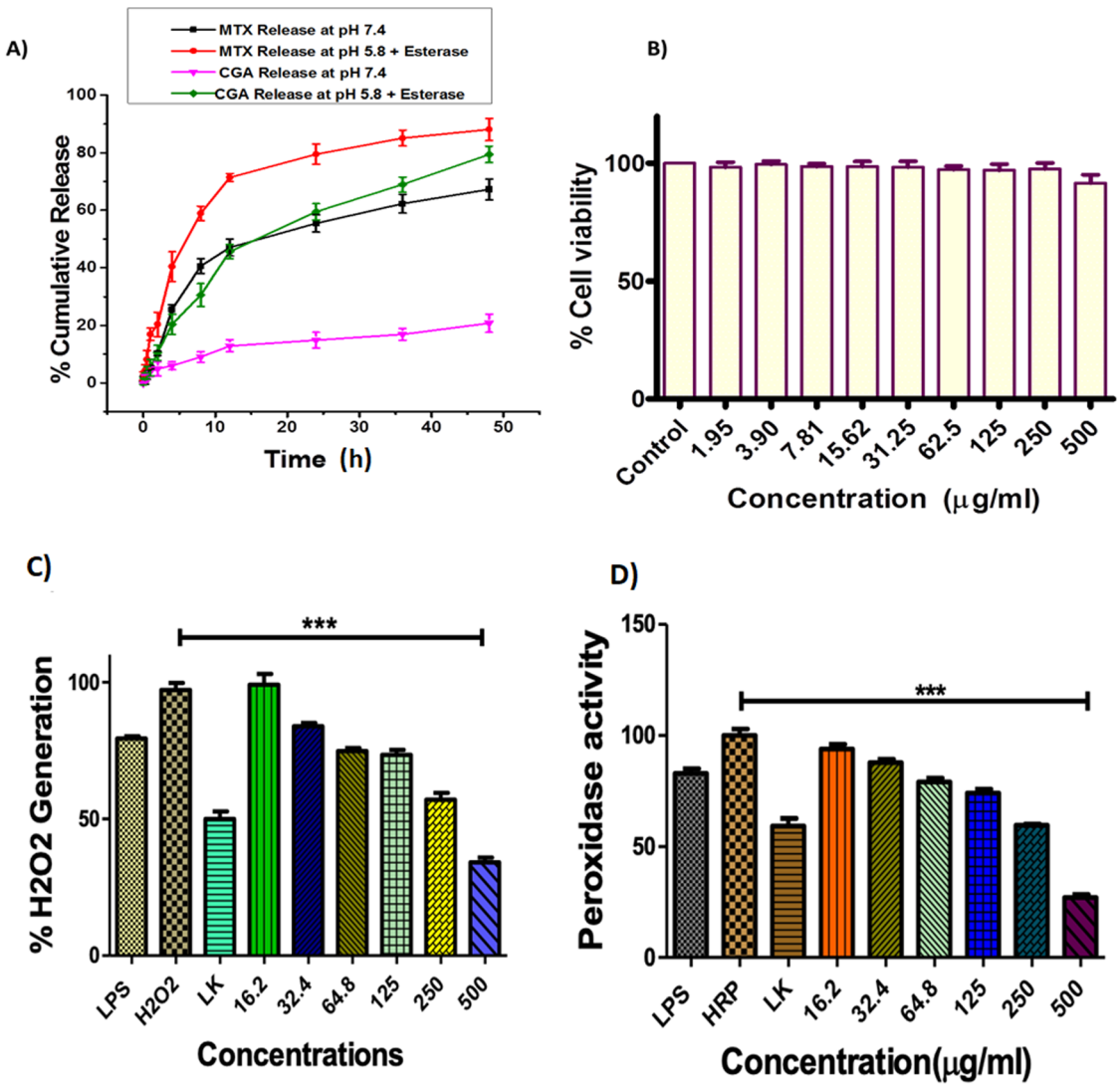

Fig. 2 Representative graphs of drug release and cytocompatibility assessment. (A) Methotrexate release from the PLGA-*b*-CGA nanomicelles. (B) Percent cell viability assessment of normal healthy human fibroblast cells hTERT BJ *versus* MTX-PLGA-*b*-CGA concentration. (C) and (D) Antioxidant parameters: H_2O_2 and peroxidase activity in the RAW264.7 cell line.

at 500 μg mL^{-1} (Fig. 2B). The antioxidant potential of MTX-loaded PLGA-*b*-CGA was also assessed against the RAW264.7 cell line (Fig. 2C and D).

Therapeutic assessment of MTX-PLGA-*b*-CGA in collagen-induced arthritis model

The anti-arthritic or anti-inflammatory effects of the MTX-PLGA-*b*-CGA nanomicelles were evaluated in collagen-induced arthritis in a Wistar rat model, as presented schematically in Fig. 3.[28,29] First, we induced arthritis in Wistar rats by immunisation with an emulsion containing collagen type II and complete Freund's adjuvant (CFA). After 14 days, full-blown arthritis symptoms were observed, and we started the treatment with the MTX-PLGA-*b*-CGA nanomicelles *via* intra-articular administration. The treatment was continued for 21 days. We evaluated the potential of the MTX-PLGA-*b*-CGA nanomicelles based on various parameters. We monitored the animals for body weight changes and compared the body weight changes among the different animal groups. We observed significant changes in body weight in the CIA group as the disease progressed. The inflammatory changes and pain in joints were responsible for reduced food intake as time proceeded, which resulted in the decreased body weight. While the CIA + MTX-PLGA-*b*-CGA group showed decreased in body weight during the disease induction and progression periods, after treatment with MTX-PLGA-*b*-CGA the body weight was observed to recover as the treatment proceeded, and at 21 days, the body weight was significantly changed or restored as compared to the CIA group and comparable with the control group. We also compared the changes in body weight in the blank PLGA-*b*-CGA and CIA + MTX groups; we observed that the changes were significant as compared to the CIA group (Fig. 4A). We assessed disease severity *via* paw diameter changes measured using Vernier calipers. We observed changes in the paw diameter in the case of the CIA group, which showed increased paw diameter due to erythema and edema in the paw. Full-blown symptoms and paw swelling were observed on day 14 and continued through day 21. Swelling and increased paw diameter were observed in the CIA + MTX-PLGA-*b*-CGA group until day 14, whereas after treatment started on day 14, the symptoms began to subside, and at day 21, the paw diameter was comparable with that of control group, which was significantly reduced compared to that of CIA group. We also compared the changes in severity with CIA *vs.* CIA + PLGA-*b*-CGA and MTX-PLGA-*b*-CGA. We observed that both the groups showed reduced arthritis severity in terms of reduced paw diameter (Fig. 4B).

We further visualized paw swelling, edema and joint damage *via* physiological visualization and X-ray assessment. We visualized the joints from different groups by positioning

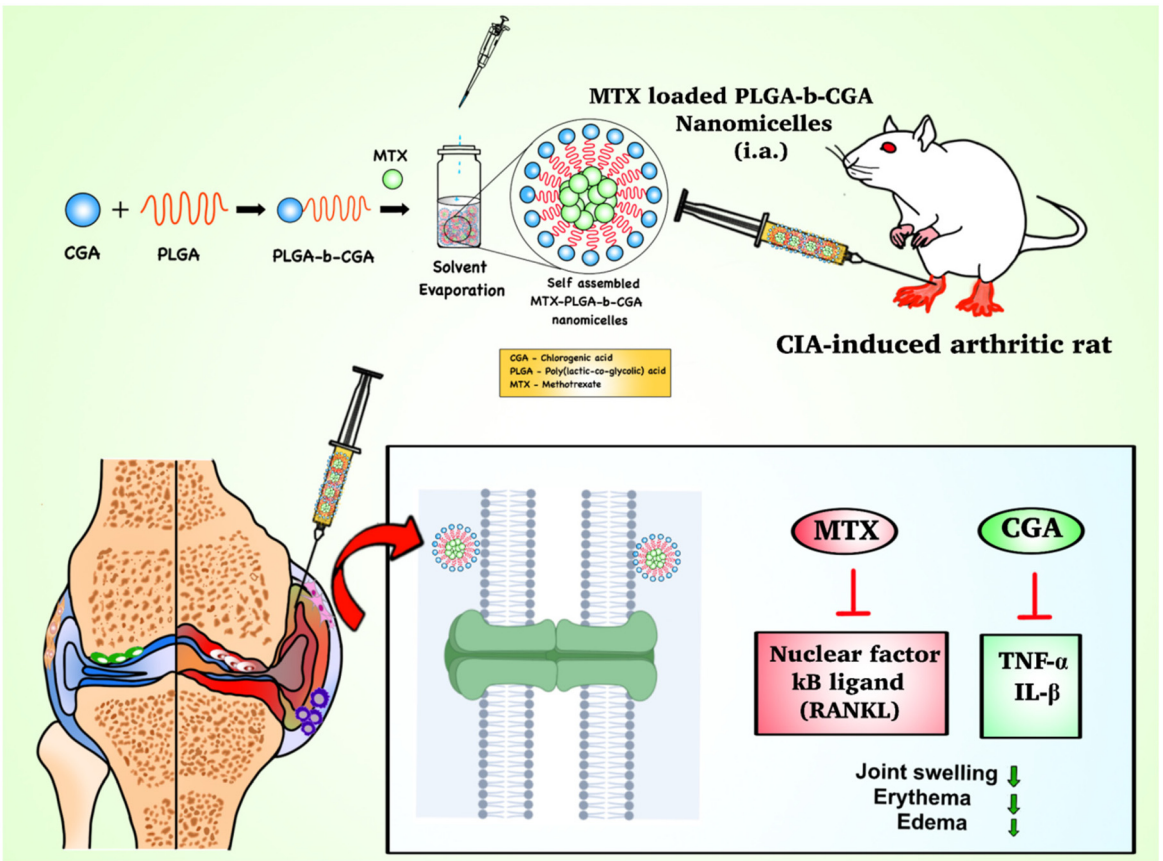

Fig. 3 Schematic illustration of the administration and therapeutic action of the MTX-PLGA-*b*-CGA nanomicelles against the collagen-induced arthritis model.

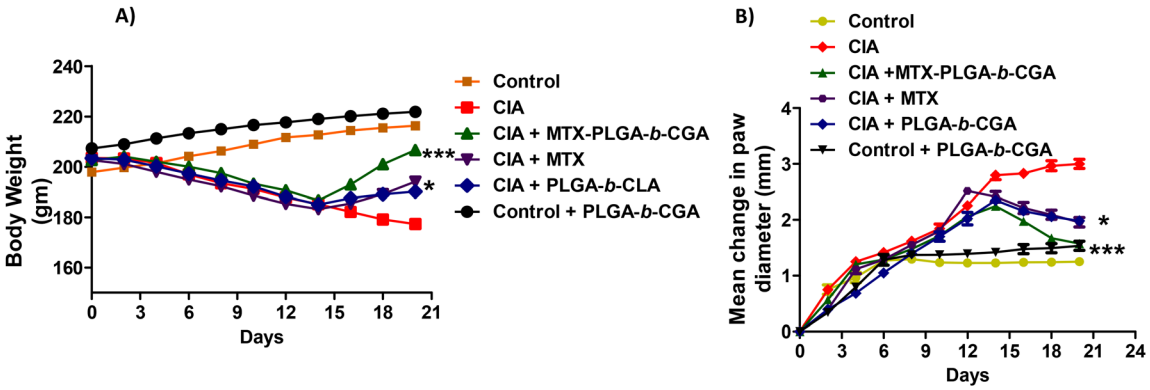

Fig. 4 Graphical representation of (A) Body weight and (B) Mean change in the paw diameter. Values are represented as mean ± SD, $N = 3$, ***/### $p < 0.001$, ** $p < 0.01$, * $p < 0.05$.

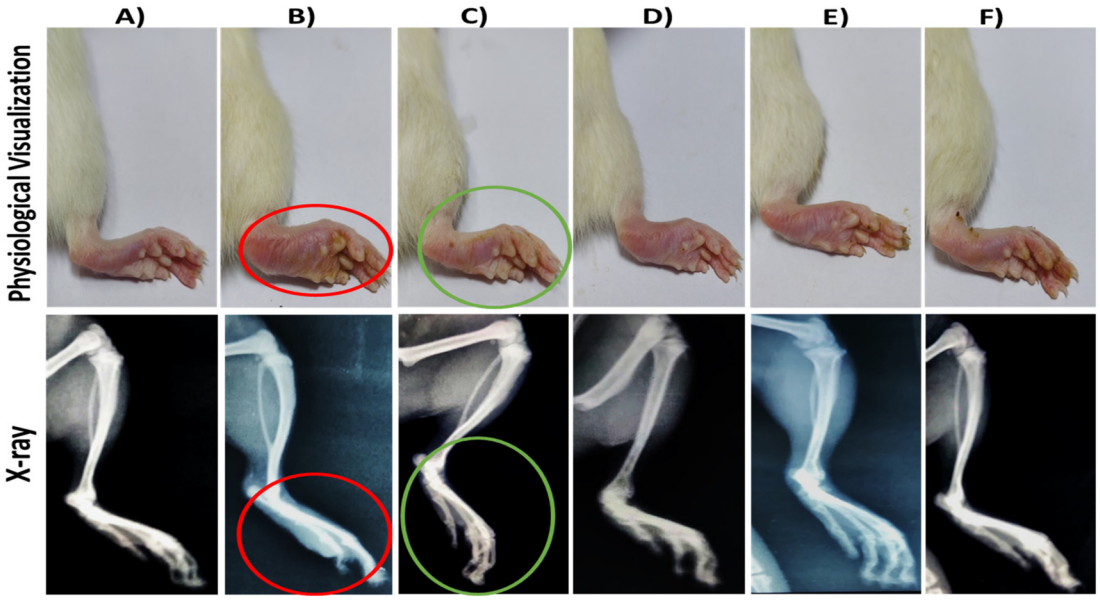

Fig. 5 Illustrative images of the joints captured on the last day of the study. Upper panels present physiological visualization of the rat joints. Lower panels present the X-ray images of rat hind paw joints. (A) – Control, (B) – CIA, (C) – CIA + MTX-PLGA-*b*-CGA, (D) – CIA + M, (E) – CIA + PLGA-*b*-CGA, (F) – Control + PLGA-*b*-CGA. $N = 3$ animals for each representative image.

the joint part with a mobile camera; rat joints were clicked on the last day of the study. We observed that the CIA group showed joint swelling as well as paw edema, visualized by redness on the hind paw (Fig. 5B). We compared the joints of the CIA + MTX-PLGA-*b*-CGA group with those of the CIA group, which showed a reduction in joint swelling as well as paw edema and redness (Fig. 5A). We also compared the swelling of the CIA + MTX and CIA + PLGA-*b*-CGA groups with that of the CIA group and observed that the joints showed relatively less swelling, redness and edema (Fig. 5D and E). We further performed X-ray analysis and observed that the CIA group animal joints showed joint stiffness and reduced articular cartilage; the joint swelling was also observed from the shadow of the swollen joint on the X-ray film (Fig. 5B). The X-ray results for the CIA + MTX-PLGA-*b*-CGA treated group showed a reduction in joint stiffness, swelling and cartilage erosion (Fig. 5C). The swelling was also found to be reduced as compared to the CIA group. We also found that CIA + PLGA-*b*-CGA and CIA + MTX showed relatively less joint stiffness, cartilage erosion, and paw erythema as compared to the CIA group (Fig. 5D and E).

Histological findings

Hematoxylin and eosin (H&E) staining was also carried out to better comprehend histological alterations. The CIA group demonstrated significantly less articular cartilage damage, more articular cartilage degradation, and less synovial gap in the joint (Fig. 6B). In contrast, following treatment with

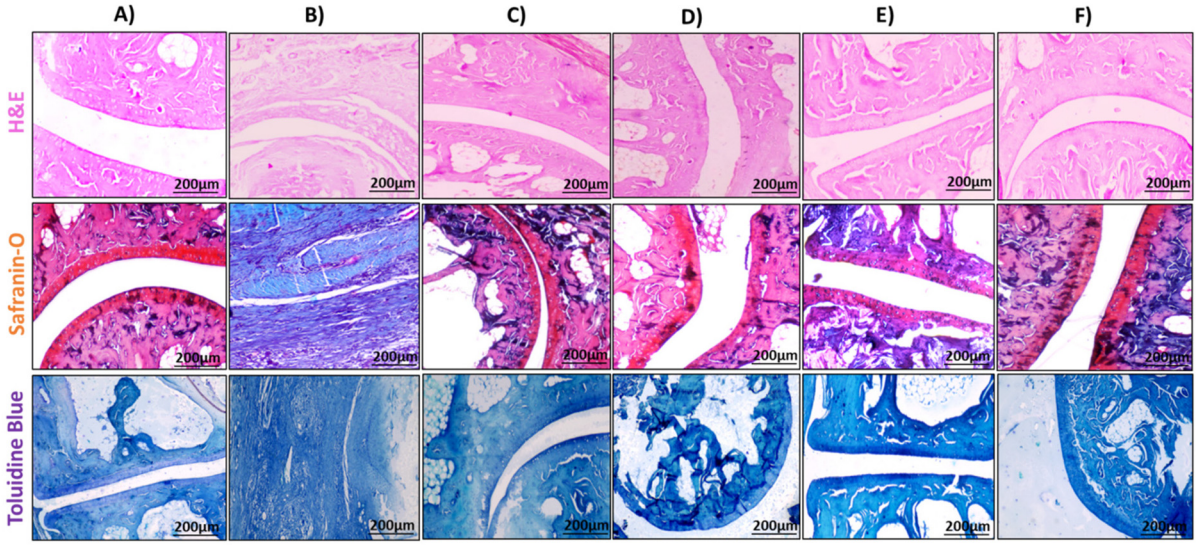

Fig. 6 Illustrative images of histological staining of rat paw joints. Upper panels present the hematoxylin and eosin staining of the histological sections from the different treatment groups. Middle panels present the safranin-o staining in the different joint histological sections. Lower panels present the toluidine blue staining for the rat joint histological sections. (A) – Control, (B) – CIA, (C) – CIA + MTX-PLGA-*b*-CGA, (D) – CIA + M, (E) – CIA + PLGA-*b*-CGA, (F) – Control + PLGA-*b*-CGA. *N* = 3 number of sections and *N* = 5 animals per group.

M-PLGA-*b*-CGA, the articular cartilage thickness appeared to be restored, and the breakdown of cartilage was observed to be reduced (Fig. 6C). Similar observations were found in the CIA + M and CIA + PLGA-*b*-CGA groups, including minor articular cartilage restoration, less degradation of cartilage, and the development of trabeculae (Fig. 6D and E). Proteoglycan is abundantly present in the matrix of healthy cartilage, but it deteriorates under arthritis conditions. We used safranin-O staining to visualize proteoglycan on histological sections. The control group showed strong staining (red), which shows that the cartilage is healthy and undamaged (Fig. 6A). The CIA group showed a noticeable decrease in the red colour of safranin-O, which indicates decreased cartilage proteoglycan due to the onset of arthritis (Fig. 6B).[28,30–32] Because of articular cartilage erosion, it was found that the cartilage thickness had decreased. There was obvious indication that M-PLGA-*b*-CGA restored the diminished proteoglycan level of the cartilage lining (Fig. 6C) (red staining). In terms of histopathological alterations, the CIA + M and CIA + PLGA-*b*-CGA (Fig. 6D and E) groups also displayed minor restoration of proteoglycan levels. We also demonstrated the proteoglycan content using toluidine blue staining. The staining findings were found to be equivalent to those in safranin-O staining. Comparing the CIA group to the M-PLGA-*b*-CGA group, which displayed a decreased proteoglycan level and staining in articular cartilage, we observed that the M-PLGA-*b*-CGA group had a considerable increase in the proteoglycan level (Fig. 6C).

Expression studies

In earlier performed research findings, chlorogenic acid (CGA) and methotrexate (MTX) were reported to act *via* the inhibition of TNF-α and RANKL.[14,33,34] We performed immunohistochemistry analysis to demonstrate the mechanism of the suppression of the inflammation. We found that the TNF-α and RANKL activity was normal in the control and control + PLGA-*b*-CGA groups (Fig. 7A and F). In contrast, in the CIA group, the level of expression was elevated, along with increased number of TNF-α and RANKL-positive cells (Fig. 7B). We further observed that the administration of M-PLGA-*b*-CGA led to a significantly reduced number of TNF-α and RANKL immunopositive cells (Fig. 7C). The simultaneous effects of the CGA and M treatments in the CIA + M-PLGA-*b*-CGA group significantly suppressed the TNF-α and RANKL expression. Compared to those of the CIA group, the levels of expression of TNF-α and RANKL were observed to be lowered in the CIA + PLGA-*b*-CGA group as well as in the CIA + M group (Fig. 7D and E). In accordance with several investigations, inflammation and deterioration of articular cartilage are associated with one another.[35] We infer that the MTX-encapsulated PLGA-*b*-CGA nanomicelles suppressed the expression of TNF-α and RANKL after analysing IHC results for many specific markers (Fig. 7). It reduced the inflammation and ultimately protected the articular cartilage from deterioration.

Inflammatory circumstances were majorly regulated by the mast cell proliferation or infiltration in tissue regions, which are involved in triggering the inflammatory response process *via* the degranulation of cells by releasing various inflammatory mediators such as histamine and other cytokines.[30,31] To determine whether mast cells were involved in inflammatory arthritis, we also carried out staining using toluidine blue to visualize the mast cells for the different groups. We observed that the CIA group had more mast cells infiltrating arthritic joints, which were visible as a dark purplish blue colour (Fig. S2B†), while the CIA + M-PLGA-*b*-CGA group showed hardly any mast cells. In comparison to the CIA group, the CIA + M and CIA + PLGA-*b*-CGA groups similarly exhibited a

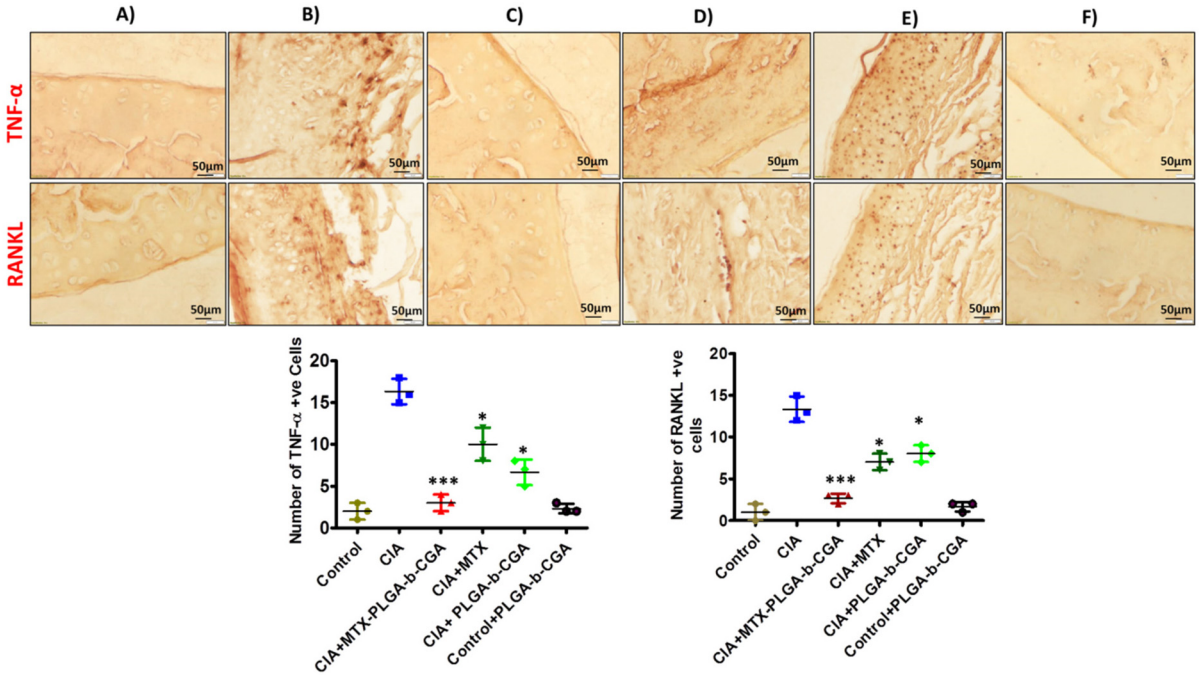

Fig. 7 Immunohistochemistry staining of the histological sections of the rat paw joints for expression analysis of TNF-α and RANKL. Lower panels express the quantification of TNF-α and RANKL positive cells in articular cartilage lining. (A) – Control, (B) – CIA, (C) – CIA + MTX-PLGA-*b*-CGA, (D) – CIA + M, (E) – CIA + PLGA-*b*-CGA, (F) – Control + PLGA-*b*-CGA. *n* = 3 number of sections and *N* = 5 animals per group.

reduced number of the mast cells. This demonstrates that the M-PLGA-*b*-CGA group significantly decreased inflammation and the number of the mast cells (Fig. S1†).

Safety assessment

We carried out H&E staining of the key organs of the control, control + PLGA-*b*-CGA, and CIA + M-PLGA-*b*-CGA groups to examine the safety of blank nanomicelles and NMs loaded with methotrexate. We collected, among other important organs, the heart, lungs, kidney, spleen, and liver. In comparison to the healthy control group, we noted that neither the control + PLGA-*b*-CGA nor CIA + M-PLGA-*b*-CGA groups had any histoarchitectural changes in any of the major organs. We observed that the blank nanomicelles we used were biocompatible and reliable for administration in experimental arthritis model rats (Fig. 8).

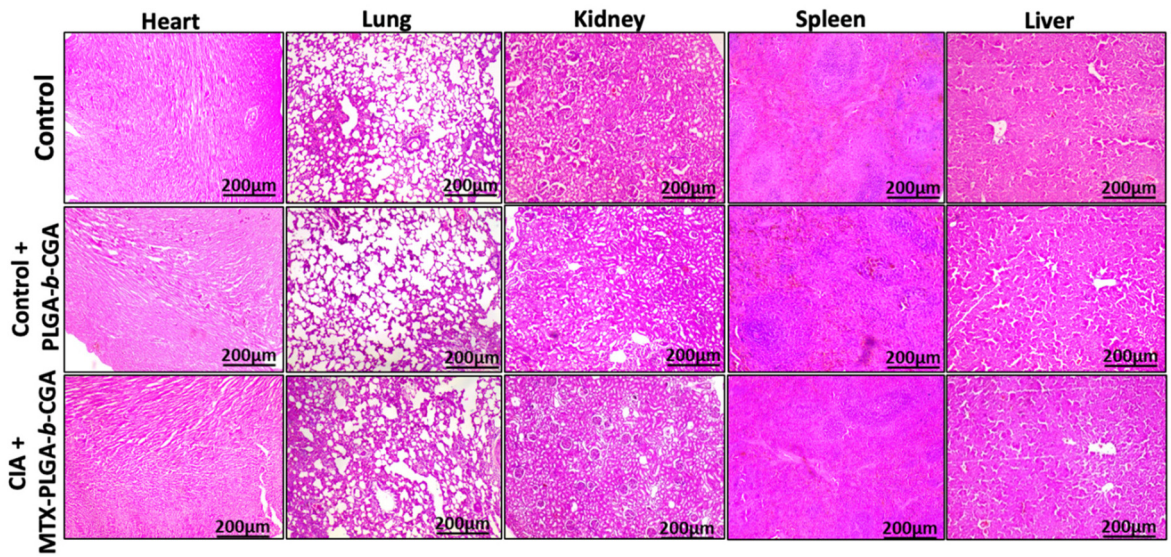

Fig. 8 Histological sections of vital organs (heart, lungs, kidneys, spleen, and liver) after treatment with M-PLGA-*b*-CGA and PLGA-*b*-CGA. *n* = number of sections, *N* = 5 animals per group.

Conclusion

Developing a drug delivery system with therapeutic advantages and drug release in a controlled manner to exert an anti-inflammatory effect is a major challenge. Herein, we developed nanomicelles conjugated with an active moiety and incorporating methotrexate (MTX) as a potent drug to provide an enhanced therapeutic effect against an experimental arthritis model. We synthesized chlorogenic acid (CGA)-conjugated PLGA nanomicelles with sizes ranging from 90–110 nm. We evaluated the therapeutic potential of the nanomicelles in a collagen-induced arthritis preclinical model and observed that the combined potential of MTX and CGA provided an enhanced therapeutic outcome by suppressing joint damage, synovial hyperplasia, cartilage erosion and joint inflammation. We elucidated potential markers and observed the simultaneous inhibition of the pro-inflammatory markers RANKL and TNF-α.

Ethical statement

Female Wistar rats (200–220 g), 6–8 weeks old, were procured from central animal facility (CAF) of National Institute of Pharmaceutical Education and Research (NIPER) Mohali. Animals were kept in the animal house of the Indian Institute of Science Education and Research, (IISER) Mohali. The standard conditions were maintained, and the experiments were carried according to IAEC and CPCSEA guidelines. Before the start of the study, the animals were acclimatised for six days. The IAEC approval number for this project is IISERM/SAFE/PRT/2023/008.

Abbreviations

MTX	Methotrexate
PLGA	Poly(L-lactide-*co*-glycolide)
CGA	Chlorogenic acid
RANKL	Receptor activator of nuclear factor kappa beta
TNF-α	Tumor necrosis factor-alpha
IL-1β	Interleukin-1 beta
OCPs	Osteoclast precursors
DAB	(3,3′-Diaminobenzidine).

Author contributions

Akshay Vyawahare: investigation, experimentation, methodology, analysis, writing – original draft. Chandrashekhar Jori: experimentation, methodology, analysis. Jattin Kumar: experimentation, Kanika: experimentation, methodology. Mohammad Fareed: writing – review & editing, Nemat Ali: writing – review & editing and analysis, Kaushik Parida: experimentation, analysis. Rehan Khan: conceptualization, writing – original draft, writing – review & editing, supervision, funding acquisition.

Conflicts of interest

The author declares no conflict of interest.

Acknowledgements

This work is supported by the Department of Science and Technology (DST), SERB with Grant No. CRG/2019/004018. The authors acknowledge and extend their appreciation to the Researchers Supporting Project Number (RSPD2024R940), King Saud University, Riyadh, Saudi Arabia.

References

1 J. S. Smolen, D. Aletaha and I. B. McInnes, *Lancet*, 2016, **388**, 2023–2038.
2 L. Klareskog, A. I. Catrina and S. Paget, *Lancet*, 2009, **373**, 659–672.
3 I. B. McInnes and G. Schett, *N. Engl. J. Med.*, 2011, **365**, 2205–2219.
4 F. A. H. Cooles and J. D. Isaacs, *Curr. Opin. Rheumatol.*, 2011, **23**, 233–240.
5 V. Taneja, in *The Autoimmune Diseases (Sixth Edition)*, ed. N. R. Rose and I. R. Mackay, Academic Press, 2020, pp. 467–489.
6 M. Zamanpoor, *Clin. Genet.*, 2019, **95**, 547–557.
7 L. Liu, F. Hu, H. Wang, X. Wu, A. S. Eltahan, S. Stanford, N. Bottini, H. Xiao, M. Bottini, W. Guo and X.-J. Liang, *ACS Nano*, 2019, **13**, 5036–5048.
8 Y. He, R. Li, J. Liang, Y. Zhu, S. Zhang, Z. Zheng, J. Qin, Z. Pang and J. Wang, *Nano Res.*, 2018, **11**, 6086–6101.
9 Q. Wang, Y. Li, X. Chen, H. Jiang, Z. Zhang and X. Sun, *Nano Res.*, 2019, **12**, 421–428.
10 G. Adami and K. G. Saag, *Curr. Rheumatol. Rep.*, 2019, **21**, 34.
11 S. Bua, L. Di Cesare Mannelli, D. Vullo, C. Ghelardini, G. Bartolucci, A. Scozzafava, C. T. Supuran and F. Carta, *J. Med. Chem.*, 2017, **60**, 1159–1170.
12 Q. Feng, J. Xu, K. Zhang, H. Yao, N. Zheng, L. Zheng, J. Wang, K. Wei, X. Xiao, L. Qin and L. Bian, *ACS Cent. Sci.*, 2019, **5**, 440–450.
13 D. M. Schwartz, Y. Kanno, A. Villarino, M. Ward, M. Gadina and J. J. O'Shea, *Nat. Rev. Drug Discovery*, 2017, **16**, 843–862.
14 A. Vyawahare, A. Ahmad, N. Kanika, A. Ali, P. Saha, V. Gowd and R. Khan, *Mater. Adv.*, 2022, 3820–3834.
15 D. Aletaha and J. S. Smolen, *JAMA, J. Am. Med. Assoc.*, 2018, **320**, 1360–1372.
16 J. R. Kalden, *Rheumatol. Ther.*, 2016, **3**, 31–42.
17 S. M. Tawfik, S. Azizov, M. R. Elmasry, M. Sharipov and Y. I. Lee, *Nanomaterials*, 2020, **11**, 70.

18 S. Qiu, X. Wu, Z. Li, X. Xu, J. Wang, Y. Du, W. Pan, R. Huang, Y. Wu, Z. Yang, Q. Zhou, B. Zhou, X. Gao, Y. Xu, W. Cui, F. Gao and D. Geng, *ACS Nano*, 2022, **16**, 17062–17079.
19 R. Huang, C. Zhang, Y. Bu, Z. Li, X. Zheng, S. Qiu, J. O. Machuki, L. Zhang, Y. Yang, K. Guo and F. Gao, *Biomaterials*, 2021, **277**, 121088.
20 S. Qiu, X. Wu, D. Geng, W. Pan, Z. Li, G. Wang, D. Li, C. Li, S. Feng, L. Zhu, Y. Xu and F. Gao, *Int. J. Biol. Macromol.*, 2023, **225**, 298–309.
21 P. S. Chauhan, N. K. Satti, P. Sharma, V. K. Sharma, K. A. Suri and S. Bani, *Phytother. Res.*, 2012, **26**, 1156–1165.
22 S. C. Kwak, C. Lee, J. Y. Kim, H. M. Oh, H. S. So, M. S. Lee, M. C. Rho and J. Oh, *Biol. Pharm. Bull.*, 2013, **36**, 1779–1786.
23 Y. Yao, C. Z. Ding and Y. Fang, *Rheumatol. Int.*, 2013, **33**, 1845–1853.
24 R. Prakash, A. Vyawahare, R. Sakla, N. Kumari, A. Kumar, M. M. Ansari, N. Kanika, C. Jori, A. Waseem, A. J. Siddiqui, M. A. Khan, A. A. B. Robertson, R. Khan and S. S. Raza, *ACS Nano*, 2023, **17**, 8680–8693.
25 Y. Kim, E. J. Park, T. W. Kim and D. H. Na, *Pharmaceutics*, 2021, **13**, 1–23.
26 R. K. Mishra, A. Ahmad, A. Kumar, A. Vyawahare, S. S. Raza and R. Khan, *Mater. Sci. Eng., C*, 2020, **116**, 111103.
27 L. Suo, C. Liu, Q.-Y. Zhang, M.-D. Yao, Y. Ma, J. Yao, Q. Jiang and B. Yan, *Theranostics*, 2022, **12**, 277–289.
28 A. Vyawahare, R. Prakash, C. Jori, A. Ali, S. S. Raza and R. Khan, *ACS Nano*, 2022, **16**, 18579–18591.
29 M. M. Ansari, A. Ahmad, R. K. Mishra, S. S. Raza and R. Khan, *ACS Biomater. Sci. Eng.*, 2019, **5**, 3380–3397.
30 L. D'Ignazio, D. Bandarra and S. Rocha, *FEBS J.*, 2016, **283**, 413–424.
31 Y. Xu and G. Chen, *Mediators Inflammation*, 2015, 246126.
32 A. Vyawahare, M. M. Ansari, A. Kumar, A. Ahmad, R. K. Mishra, C. Jori, A. Nadeem, N. Siddiqui, S. S. Raza and R. Khan, *Life Sci.*, 2023, **334**, 122206.
33 M. Ji, H. J. Ryu, H. M. Baek, D. M. Shin and J. H. Hong, *Exp. Mol. Med.*, 2022, **54**, 503–517.
34 K. Matsuda, N. Shiba and K. Hiraoka, *Int. J. Mol. Sci.*, 2023, **24**, 5173.
35 S. S. Makarov, *Arthritis Res.*, 2001, **3**, 200–206.